Metal Electrode-Free Halide Perovskite-Based Flexible Ultraviolet-C Photodetector with Large Area

Thi My Huyen Nguyen[1], Sean M. Garner[2] and Chung Wung Bark[1*]

Abstract

Ultraviolet-C (UVC) photodetector has appealed to a numerous number of research owing to its manifold applications in wireless communication, flame monitoring, and medicine. However, in addition to superior performance and high stability of recent studies, scalability and production cost are important factors for commercialization and practical implementation. In this study, a halide perovskite-based UVC photodetector was fabricated using spin-coating process and low-temperature annealing. Corning® Willow® Glass was selected as the substrate for the bottom-illuminated device due to its flexibility and exceptional optical transmission (approximately 60%) in the deep-UV region. The device had a vertical structure with a large active area (1 cm^2) owing to the judicious utilization of electrodes. Under bent state with a curvature radius of 25 mm, the as-fabricated device exhibited high response and repeatability with an on/off ratio of 9.57×10^3, a fast response speed of 45/46 ms (rise/fall times) at zero bias under the illumination of a 254-nm UV lamp. The results are based on a flexible and lightweight photodetector without the utilization of notable metal electrodes.

Keywords: Flexible glass, Metal-free electrode, UVC photodetector, Halide perovskite

Introduction

In recent years, lead halide perovskites have attracted significant attention in the field of optoelectronics due to their several advantages such as high carrier mobility, long exciton diffusion length, high absorption coefficient, low defect density, and tunable optical bandgap [1–4]. Additionally, its wide absorption range ensures response in the range of near-infrared wavelength to X-ray region [5–7]. Broadband photodetectors based on halide perovskite can be used for multiple applications such as image sensing, wireless communication, environmental monitoring, and medicine [8–11].

Low-cost halide perovskites have been utilized for the fabrication of wearable and portable photodetectors on commercial flexible substrates owing to advantages such as low-temperature fabrication and solution processability. For example, Dingjun Wu and coauthors recently reported an MAPbI$_3$ nanowire photodetector by using welding strategy with outstanding on/off photocurrent ratio of 2.8×10^4 and high detectivity of 4.16×10^{12} Jones [12]. Another approach, by using 1-butyl-3-methylimidazolium tetrafluoroborate (BMIMBF4) as an additive in fabrication MAPbI$_3$ nanowire, the perovskite-based photodetector, exhibited not only ultrasensitive performance (specific detectivity of 2.06×10^{13} Jones) under 473 nm laser illumination but also ultrahigh stability for more than 5000 h without any encapsulation [13]. Flexible broadband photodetectors can be fabricated on commercial polymer substrates such as polyethylene terephthalate (PET), polystyrene (PS), polyethylene naphthalate (PEN), dimethylsiloxane (PDMS), and polyimide (PI)

*Correspondence: bark@gachon.ac.kr

[1] Department of Electrical Engineering, Gachon University, 1342 Seongnam-daero, Sujeong-gu, Seongnam-si, Gyeonggi-do 13120, South Korea
Full list of author information is available at the end of the article

Nguyen *et al. Nanoscale Research Letters* (2022) 17:94

Page 2 of 8

for the development of compact and lightweight devices [14–16]. However, a major drawback of these polymer materials is their limited wavelength response in the ultraviolet (UV) range. Deep-UV radiation is limited to approximately 300 nm, and the high optical absorption of substrates severely affects the device performance. In contrast, flexible Corning® Willow® Glass has a higher optical transmission in the deep-UV region [17, 18]. Hence, it can be used as an alternative to conventional flexible substrates for the development of ultraviolet–infrared (UV–IR) broadband photodetectors based on illumination through the substrate. Therefore, in this study, a device based on illumination through the substrate is developed, which can utilize the enhanced optical transmission through the substrate.

Regarding device structure, the interest in self-powered and flexible feasibility are characteristics to be considered. Addressing them, vertically-stacked devices exhibit fast electron/hole injection due to the shortening of the pathway in comparison with that of devices with a lateral structure [19]. Based on a built-in potential, photogenerated carriers can separate without the application of an external power supply. Supported by spiro-OMeTAD simultaneously functioned as an electron-blocking and a hole-transfer layer, photogenerated carriers quickly moved to the opposite electrodes to produce an electric current. Moreover, Lai et al. recently demonstrated that construction of a perovskite-based photodetector in vertical structure enables a remarkably higher mechanical flexibility than one in lateral structure [20]. In addition to the device architecture, the conductive polymer thin films are expected to be flexible electrodes with high mechanical durability to bending deformation rather than the rigid oxides (e.g., indium tin oxide, fluorine-doped tin oxide) and metal (e.g., Au, Ag, Pt) electrodes, especially for large-active area device [21]. Additionally, photodetectors are fabricated using complex methods and expensive metal electrodes such as Au, Ag, and Pt that increase the cost of production and impede large-scale production. To solve this problem, a transparent conductive polymer called poly(3,4-ethylenedioxythiophene) polystyrene sulfonate (PEDOT:PSS) is used as the photodetector electrode. Therefore, a simple spin-coating method can be used throughout the deposition process. A high-quality PEDOT:PSS thin film from an aqueous solution (PH1000) is used as the bottom electrode to allow the penetration of deep-UV light. On the top surface, a thin film obtained from the dissolution of dry re-dispersible PEDOT:PSS in isopropanol is in direct contact with the underneath layer. Therefore, the device is metal-electrode-free, flexible, and has a large active area. The bottom-illuminated device exhibited high performance in the UVC region with the self-powered operation and

bending ability. A large photocurrent of 4.76 μA was generated by the device using metal-free electrodes due to the large active area. These results demonstrate a low-cost fabrication method for the development of halide perovskite-based broadband photodetectors which can be used in various industrial and scientific fields.

Experimental

Preparation of the Top Electrode

PEDOT:PSS solution was prepared by dissolving PEDOT:PSS orgacon™ dry (Sigma-Aldrich) in isopropyl alcohol (IPA) at a concentration of 1.3 wt.%. The dispersed solution was treated within 2 h of the ultrasonication under 40% amplitude and 10 s on/10 s off of time pulse.
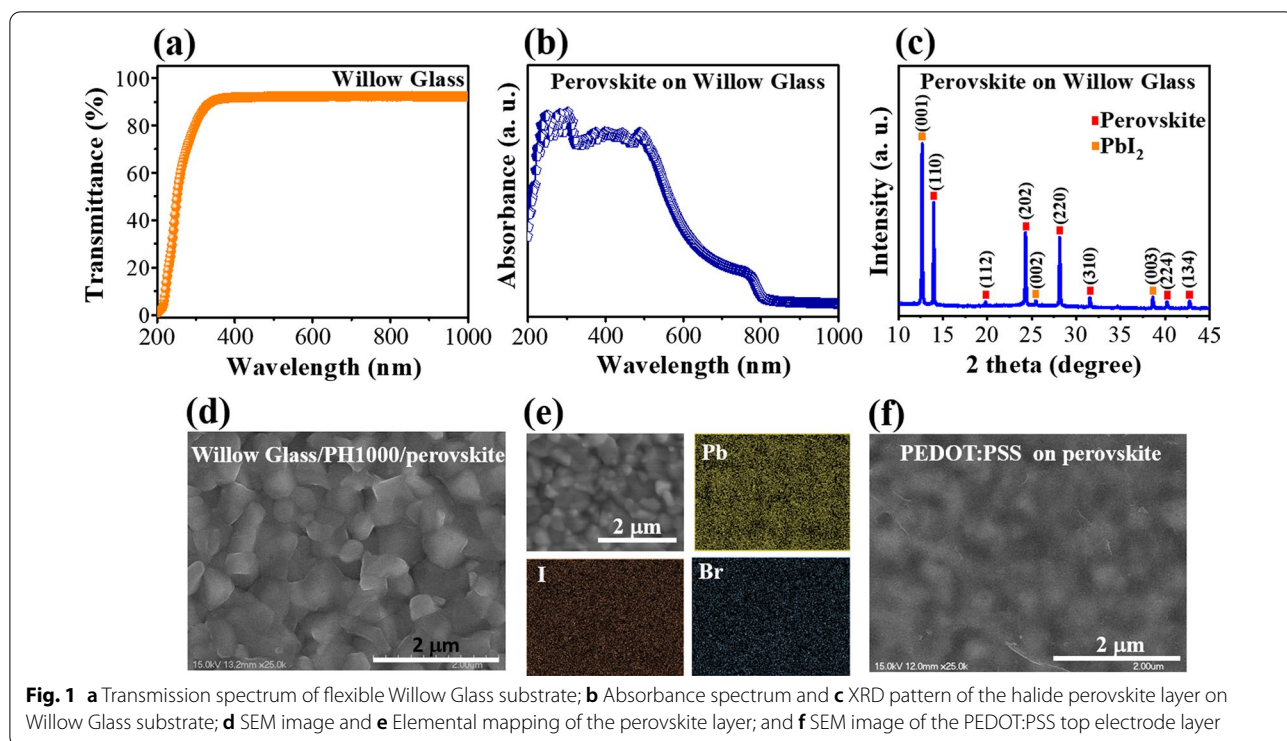
Preparation of UV Photodetector

A flexible perovskite-based UV photodetector was fabricated using a solution-based spin-coating process and annealing at low temperatures. First, a 100-μm-thick Willow Glass substrate (20 mm × 20 mm) was cleaned with acetone, deionized water, and ethanol in an ultrasonic bath for 10 min during each cycle. The substrate was dried using nitrogen gas. Subsequently, a conductive bottom electrode was deposited on the clean glass by spin-coating Clevios™ PH1000 aqueous solution. The bottom electrode was treated with methanol as reported in a previous study [22]. A UV absorber film of halide perovskite was applied to the PH1000 layer via a two-step method. In the first step, a 1.3 M PbI_2 solution in DMF:DMSO (0.95:0.5) was spin-coated at 2000 rpm for 30 s and annealed at 70 °C for 1 min. In the second step, a mixed organic halide solution which consisted of 60 mg FAI/6 mg MABr/6 mg MACl in 1 mL IPA was spin-coated on PbI_2 layer at 4000 rpm for 20 s (loading time of 20 s) and specimen was heated on a hot plate at 150 °C for 15 min to form the perovskite layer. Subsequently, a hole transport layer which consisted of 85 mg spiro-OMeTAD dissolved in 1 mL chlorobenzene, 28.8 μL 4-tert-butyl pyridine, and 17.5 μL Li-TFSI (520 mg Li-TFSI in 1 mL acetonitrile) was spin-coated onto the perovskite layer at 4000 rpm for 30 s. Finally, the top electrode was prepared by spin-coating 100 μL PEDOT:PSS solution in IPA on the surface of the spiro-OMeTAD layer at 1000 rpm for 60 s and heated at 50 °C for 5 min. Two copper wires were attached to the device using adhesive tape to connect them with the external circuit. The active area of the device was 1 cm^2. For the bending test, the device was closely attached to a piece of flat plastic to determine the curvature radius and bending angle.

Device Characterization

The crystal structure of the perovskite on the flexible glass was identified using X-ray diffraction (XRD; Rigaku DMAX 2200, Japan) with Cu Kα radiation ($\lambda = 1.506$ Å) in the 2θ range of 10°–45° and a scan rate of 5° min^{-1}. The transmittance of 100-μm-thick Willow Glass in the deep-UV region and the absorption of the perovskite film on the substrate were measured using an ultraviolet–visible spectroscopy system (UV–Vis; Agilent 8453, USA). The recombination of electron−hole pairs in the perovskite was determined using a steady-state photoluminescence spectrometer (PL; QuantaMaster TM 50 PTI, USA) in the wavelength range of 750–800 nm with light excitation at 520 nm. The top views of perovskite film, PEDOT:PSS film on perovskite, and the cross-sectional images of the device were captured using scanning electron microscopy (SEM; S-4700, Hitachi, Japan) and a focused ion beam SEM system (FEI Nova Nanolab 200, USA), respectively. The electrical conductivities of two electrodes were measured by using a four-point probe system (Advance Instrument Technology, CMT SR-2000N). The spectral response was measured using the analyzer equipment (Keithley 2400 SourceMeter, USA) with a UV lamp (VL6.LC, France) as the light source.

Results and Discussion

The morphology, crystal structure, and optical properties of the halide perovskite-based UV photodetector are shown in Fig. 1. The transmission range of wavelengths in the range of 190–1000 nm for the 100-μm-thick Willow Glass is depicted in Fig. 1a. It can be observed that the transmittance was approximately 60% at a wavelength of 254 nm. Accordingly, UVC radiation in the range of 100–280 nm can pass through the flexible glass substrate to the active layer. The ultraviolet–near-infrared (UV–NIR) optical absorption of halide perovskite material on Willow Glass substrates is presented in Fig. 1b. The spectrum exhibits good absorption, particularly in the deep-UV region. The absorption of halide perovskite is consistent with the results obtained in previous studies [23–25]. Additionally, the XRD pattern of the absorbing layer (Fig. 1c) shows a set of prominent diffraction peaks at 2θ: 13.98, 19.81, 24.29, 28.19, 31.53, 40.26, and 42.8° corresponding to planes of (110), (112), (202), (220), (310), (224), and (134), respectively, that demonstrate the formation of the crystallographic phase of perovskite material on the Willow Glass [26–30]. The surface morphology of the active layer on flexible glass can be examined by the top-view SEM image and elemental mapping shown in Fig. 1d–e. A continuous and smooth film with large grains of perovskite crystals and a uniform distribution of Pb, I, and Br elements in the component layer can be observed in the figure. Furthermore, the surface

Fig. 1 a Transmission spectrum of flexible Willow Glass substrate; **b** Absorbance spectrum and **c** XRD pattern of the halide perovskite layer on Willow Glass substrate; **d** SEM image and **e** Elemental mapping of the perovskite layer; and **f** SEM image of the PEDOT:PSS top electrode layer

Nguyen *et al. Nanoscale Research Letters*   (2022) 17:94

Page 4 of 8

of the top electrode can be clearly observed in the SEM image in Fig. 1f. It confirms a 100% surface coverage on the prior layer by the prepared PEDOT:PSS solution via a simple spin-coating method.

Figure 2a–c illustrates the schematic diagram, cross-sectional image, and a photograph of the photodetector device, respectively. It can be observed that the halide perovskite-based photodetector was constructed on a flexible Willow Glass with conductive polymer electrodes using two different types of solutions PH1000 aqueous solution (for the bottom electrode) and PEDOT:PSS slurry (for the top electrode). The layers of the components and the thicknesses can be observed in Fig. 2b. The thickness of the perovskite and PH1000 layers was ~564 nm and ~82.5 nm, respectively. Furthermore, the layers of spiro-OMeTAD and PEDOT:PSS were complicated to distinguish because they have a good contact [35]. The top electrode layer can be determined due to the presence of a few defects that can be observed on a large scale. These defects were observed because PEDOT:PSS arrays were stacked on top of each other. The electrical conductivity values of PH1000 film and PEDOT:PSS film are 1032 and 223 S cm^{-1}, respectively, suggesting efficient charge transport in the role of electrodes for the device. The energy diagram shown in Fig. 2c can be used to understand the mechanism of the photodetector fabricated on the flexible substrate. Upon the illumination of UV radiation, the energy penetrates through the transparent bottom electrode toward an active perovskite absorber layer. The electrons and holes are separated and self-driven to opposite sides. Owing to the built-in electric field and corresponding energy levels in the device, the photodetector can operate in the absence of a bias voltage. Furthermore, the two copper wires circulate the charge carriers through the external circuit to form current signals. Therefore, the self-powered photodetector can operate in a large active area without the requirement of thermal evaporation of noble metal electrodes such as Ag, Au, and a large amount of photocurrent was generated.

The calculations and images shown in Fig. 3a and b, respectively, can be used to evaluate the performance of the photodetector on the flexible glass substrate during bending. The photodetector with a size of 20 mm × 20 mm was attached to a piece of plastic using tape. When the plastic was bent, the sample was bent as well. At the bending threshold (before breaking), the size of the sample under bending was measured to be 20 mm × 19.05 mm, and the height (distance between straight and bending) was measured to be 0.565 mm. Subsequently, a circular arc (black dash line) was fitted to overlap the sample arc under bending (blue dash arc). The bending angle and curvature radius were determined by drawing two tangents to the circle (red dash lines) and were equal to 40° and 25 mm, respectively. It can be observed in Fig. 3c that the photoresponse of the device exhibited stability and flexibility after repeatedly bent for 200 cycles at a fixed bending angle of 40°. This result
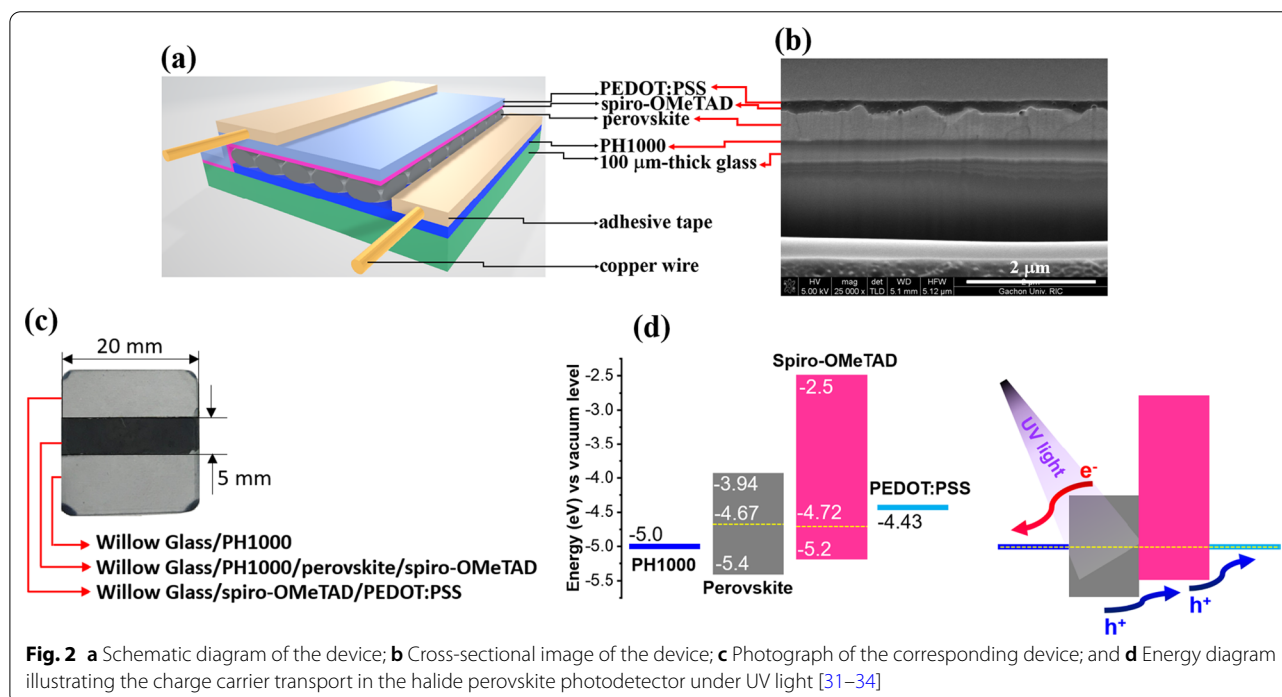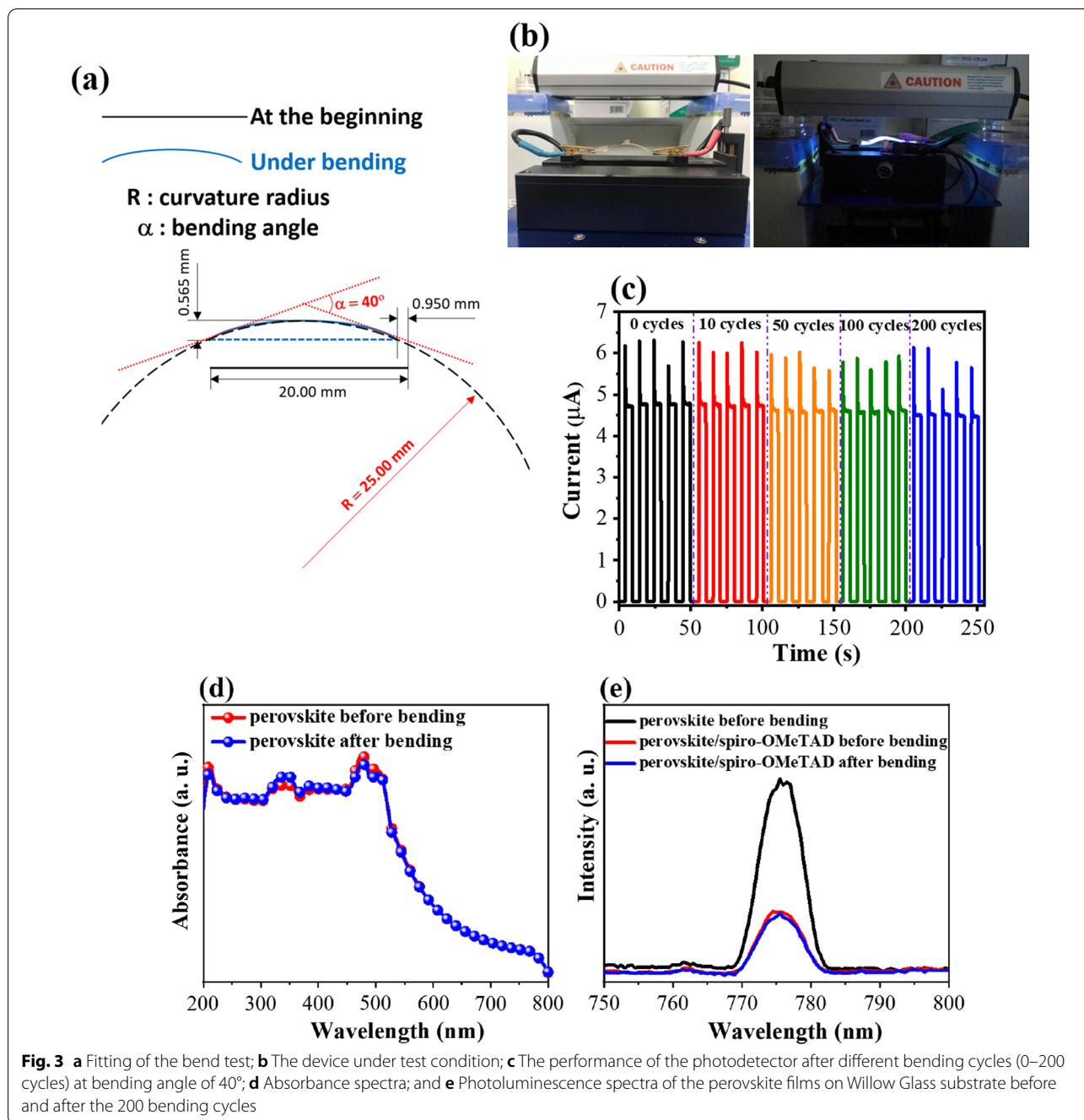

Fig. 2 **a** Schematic diagram of the device; **b** Cross-sectional image of the device; **c** Photograph of the corresponding device; and **d** Energy diagram illustrating the charge carrier transport in the halide perovskite photodetector under UV light [31–34]

Nguyen *et al. Nanoscale Research Letters*   (2022) 17:94

Page 5 of 8

Fig. 3 **a** Fitting of the bend test; **b** The device under test condition; **c** The performance of the photodetector after different bending cycles (0–200 cycles) at bending angle of 40°; **d** Absorbance spectra; and **e** Photoluminescence spectra of the perovskite films on Willow Glass substrate before and after the 200 bending cycles

demonstrated that the layers were not affected by the bending process at a moderate angle. The high mechanical durability was owing to the vertical construction of device [20]. Unlike the flexible polymer electrodes, the perovskite film can be cracked under tension during bending, which creates more surface defects to impede the transport of photogenerated charges toward electrodes in the horizontal direction. However, the negative influence of these defects on charge transfer will be suppressed because the charge carriers in the active area transfer to electrodes in the vertical direction. It is noted that thickness of the perovskite photoabsorber (~450 nm, Fig. 2b) is considered as the pathway of photogenerated charges in vertical direction. Indeed, the UV–Vis spectra of the perovskite layer on Willow Glass (Fig. 3d) measured at the beginning and after 200 bending cycles showed a similar absorption intensity, indicating maintenance of the optical property of the absorber

Nguyen *et al. Nanoscale Research Letters*   (2022) 17:94

Page 6 of 8

material. Moreover, the PL measurements (Fig. 3e) were conducted to examine the effect of bending on carrier transport in the perovskite layer. In particular, the emission peak at 775 nm was assigned to the electron–hole recombination in the perovskite layer when it is under a light excitation of 520 nm. By using a hole transport layer of spiro-OMeTAD, photogenerated holes in the perovskite can move quickly to the spiro-OMeTAD side leading to reduce the band-to-band charge recombination, thus resulting in a significant reduction of PL peak intensity. Notably, the similarity of intensity was observed for devices after bending, indicating the unchanged charge transport in the as-prepared device before and after bending.

The UVC response of the device at various incident light intensities was evaluated under the bent state. As depicted in Fig. 4a, the photocurrent generated increased monotonously with the power intensities from 0.354 to 0.774 mW/cm^2 in the self-powered mode. The maximum value of photocurrent generated by the device was 4.76 μA, and it had a fast rise time of 45 ms and it returned to the initial dark current within 46 ms (Fig. 4b). Herein, the rise/fall time (t_{rise}/t_{fall}) is defined as the period from 10 to 90% of the peak value and from 90 to 10% of the peak value, respectively [23]. This response time as well as other critical parameters of our device are comparable

with many reported flexible UV photodetectors in Table 1. Furthermore, Fig. 4c and d displays a reproducible and stable photoresponse of the device under multiple periodic on/off operations. In detail, the detector exhibited reproducibility during 500 consecutive on/off cycles accompanied by photostability under continuous 254 nm illumination up to 500 s. A quantitative assessment of self-powered photodetector was presented using two key parameters, responsivity (R) and specific detectivity (D^*). They were expressed as $R = (I_{light} − I_{dark})/P_{opt}S$ and $D^* = R/(2qJ_{dark})^{1/2}$, where I_{light} is the current under 254-nm UV illumination, and I_{dark} and J_{dark} are the dark current and dark current density, respectively. P_{opt} is the incident optical intensity, q is the electron charge, and S is the effective device area (1 cm^2) [36, 37]. The values of R and D^* were calculated at different light intensities using the two above-mentioned equations and are plotted in Fig. 4e. A slight decrease in the curves can be observed with an increase in the power of light. The decrease was attributed to the recombination of defects present in the active area (1 cm^2). This change can be verified by the power law: $I_{light} \propto P_{opt}^{\theta}$, where θ is the index of the power exponent. As shown in Fig. 4f, this exponent was determined to be 0.87 ($\theta < 1$) for light intensity in the range of 0.354–0.774 mW/cm^2, which demonstrates the dependence of photoresponse on incident light power
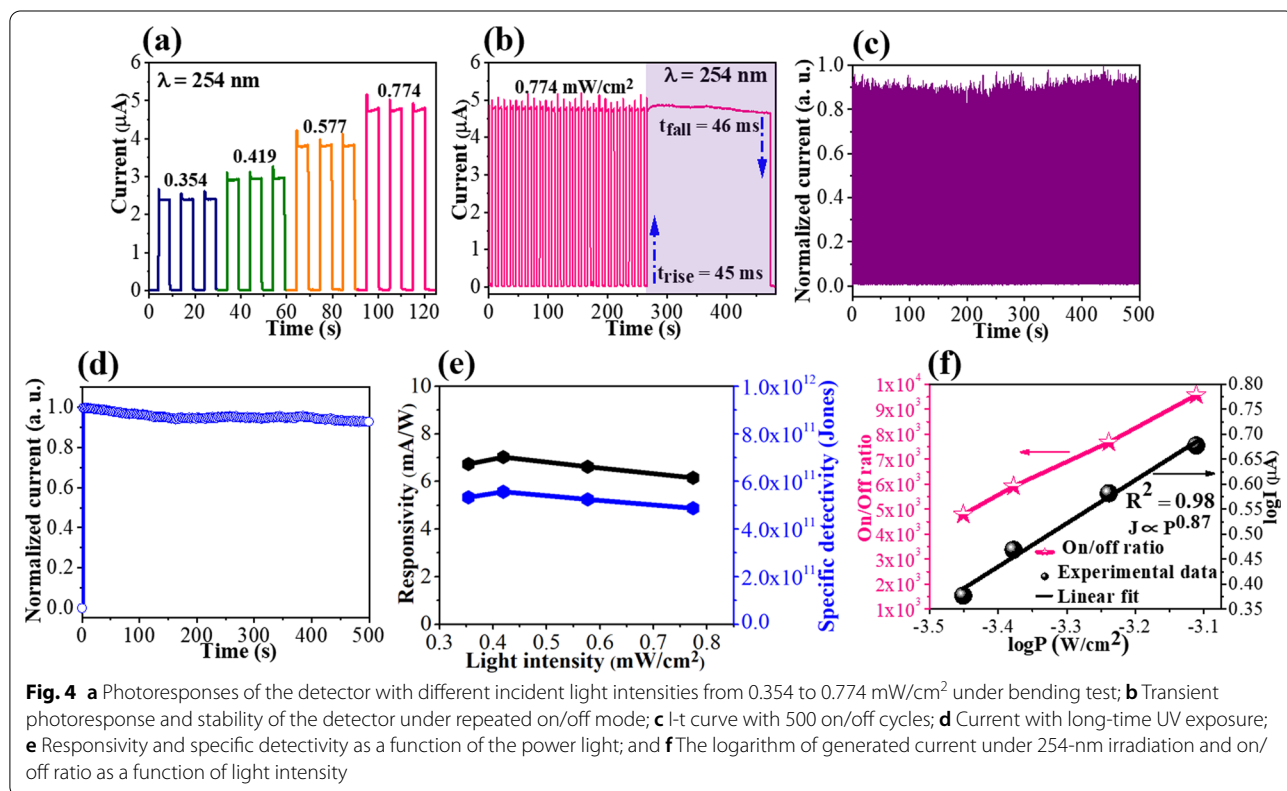

Fig. 4 **a** Photoresponses of the detector with different incident light intensities from 0.354 to 0.774 mW/cm^2 under bending test; **b** Transient photoresponse and stability of the detector under repeated on/off mode; **c** I-t curve with 500 on/off cycles; **d** Current with long-time UV exposure; **e** Responsivity and specific detectivity as a function of the power light; and **f** The logarithm of generated current under 254-nm irradiation and on/off ratio as a function of light intensity

Nguyen *et al. Nanoscale Research Letters*   (2022) 17:94

Page 7 of 8

Table 1 Performance comparisons of previous flexible photodetectors

Device structure	Bias (V)	λ (P_{opt}) [nm (mW/cm^{-2})]	I_{photo} (μA)	On/off ratio	Response time	Refs.
Willow Glass/PH1000/perovskite/spiro-OMeTAD/PEDOT:PSS	0	254 (0.774)	4.76	9.57×10^3	45/46 ms	This work
PET/ITO/TiO$_2$/PEDOT:PSS	0	254 (0.6)	0.22	220	64/106 ms	[40]
PET/Ag/(Ti core/TiO$_2$ shell) wire/Ag	-1	365 (18)	1	1.8	13.9/10.23 s	[41]
Mica/AZO/NiO/β-Ga$_2$O$_3$/ITO	2	265 (0.375)	5	10^3	80/570 ms	[42]
PET/ITO/SnO$_2$/perovskite/ITO	3	388 (11)	0.013	234	< 0.4 s	[43]
Paper/Ag/Sr$_2$Nb$_3$O$_{10}$/Ag	5	260 (0.46)	1.7	1.1×10^2		[44]
PET/MoO$_3$/Au	10	380 (200)	0.3318	3.68×10^2	0.94 s	[45]
Hair/AZO/ZnO/PVK/PEDOT:PSS	-5	365 (2.47)	5.5×10^{-3}	11	110/200 ms	[46]

caused by traps and defects [8, 38, 39]. Therefore, *R* and D^* values are proportional to $P_{opt}^{-0.13}$ and have a tendency to decrease with high intensity. Similarly, the on/off ratio has a dependence on the power of light. Furthermore, it was observed that the magnitude of current generated under UVC illumination was thrice of the dark current at the investigated intensities. Additionally, the on/off ratio increased twice (4.79×10^3–9.57×10^3) due to the large active area. This indicated that the photodetector constructed on the Willow Glass substrate has a performance comparable with that of other devices in terms of high response, flexibility, and self-powered operation.

Conclusions

A high-performance perovskite-based UVC photodetector was fabricated on a flexible Willow Glass substrate without using expensive metal electrodes. Spin-coating process and low-temperature annealing were used to fabricate the conducting polymers using two types of solutions, PH1000 (for the bottom electrode) and PEDOT:PSS (for the top electrode), to obtain a large active area. The device generated a maximum current of 4.76 μA at zero bias, and it exhibited a fast response time ($t_{rise}/t_{fall} = 45/46$ ms) and a good on/off ratio under bent state. This study demonstrated a flexible photodetector that can operate under bottom-to-top illuminated UVC light due to high transmittance (60%) of the 100-μm-thick glass.

Abbreviations

PEDOTPSS: Poly(3,4-ethylenedioxythiophene) polystyrene sulfonate; XRD: X-ray diffraction; UV–Vis: Ultraviolet–visible; SEM: Scanning electron microscope; R: Responsivity; D*: Specific detectivity; PET: Polyethylene terephthalate; PS: Polystyrene; PEN: Polyethylene naphthalate; PDMS: Dimethylsiloxane; PI: Polyimide.

Availability of Data and Materials
All data supporting the conclusions of this article are included within the article.

Declarations

Ethics Approval and Consent to Participate
Not applicable.

Consent for Publication
All authors have approved the publication of this article.

Competing interests
The authors declare that they have no competing interests.

Author details
[1]Department of Electrical Engineering, Gachon University, 1342 Seongnam-daero, Sujeong-gu, Seongnam-si, Gyeonggi-do 13120, South Korea. [2]Corning Research and Development Corporation, One River Front Plaza, Corning, NY 14831, USA.

References
1. Ka I, Gerlein LF, Asuo IM, Nechache R, Cloutier SG (2018) An ultra-broadband perovskite-PbS quantum dot sensitized carbon nanotube photodetector. Nanoscale 10:9044–9052
2. Lin Q, Armin A, Nagiri RCR, Burn PL, Meredith P (2015) Electro-optics of perovskite solar cells. Nat Photonics 9:106–112
3. Ding J, Fang H, Lian Z, Lv Q, Sun J-L, Yan Q (2018) High-performance stretchable photodetector based on CH$_3$NH$_3$PbI$_3$ microwires and graphene. Nanoscale 10:10538–10544

Nguyen *et al. Nanoscale Research Letters* (2022) 17:94

Page 8 of 8

4. Asuo IM, Fourmont P, Ka I, Gedamu D, Bouzidi S, Pignolet A et al (2019) Highly efficient and ultrasensitive large-area flexible photodetector based on perovskite nanowires. Small 15:1804150

5. Perumal Veeramalai C, Yang S, Zhi R, Sulaman M, Saleem MI, Cui Y et al (2020) Solution-processed, self-powered broadband $CH_3NH_3PbI_3$ photodetectors driven by asymmetric electrodes. Adv Opt Mater 8:2000215

6. Ding J, Fang H, Lian Z, Li J, Lv Q, Wang L et al (2016) A self-powered photodetector based on a $CH_3NH_3PbI_3$ single crystal with asymmetric electrodes. CrystEngComm 18:4405–4411

7. Yakunin S, Sytnyk M, Kriegner D, Shrestha S, Richter M, Matt GJ et al (2015) Detection of X-ray photons by solution-processed lead halide perovskites. Nat Photon 9:444–449

8. Zeng LH, Chen QM, Zhang ZX, Wu D, Yuan H, Li YY et al (2019) Multilayered $PdSe_2$/perovskite Schottky junction for fast, self-powered, polarization-sensitive, broadband photodetectors, and image sensor application. Adv Sci 6:1901134

9. Zhang Z, Zheng W, Lin R, Huang F (2018) High-sensitive and fast response to 255 nm deep-UV light of $CH_3NH_3PbX_3$ (X = Cl, Br, I) bulk crystals. R Soc Open Sci 5:180905

10. Kang CH, Dursun I, Liu G, Sinatra L, Sun X, Kong M et al (2019) High-speed colour-converting photodetector with all-inorganic $CsPbBr_3$ perovskite nanocrystals for ultraviolet light communication. Light Sci Appl 8:1–12

11. Kim H, Han JS, Choi J, Kim SY, Jang HW (2018) Halide perovskites for applications beyond photovoltaics. Small Methods 2:1700310

12. Wu D, Zhou H, Song Z, Zheng M, Liu R, Pan X, Wan H, Zhang J, Wang H, Li X (2020) Welding perovskite nanowires for stable, sensitive, flexible photodetectors. ACS Nano 14:2777–2787

13. Wu D, Xu Y, Zhou H, Feng X, Zhang J, Pan X, Gao Z, Wang R, Ma G, Tao L (2022) Ultrasensitive, flexible perovskite nanowire photodetectors with long-term stability exceeding 5000 h. InfoMat e12320

14. Kim JM, Kim S, Choi SH (2018) High-performance nip-type perovskite photodetectors employing graphene-transparent conductive electrodes N-type doped with amine group molecules. ACS Sustain Chem Eng 7:734–739

15. Wang M, Cao F, Meng L, Tian W, Li L (2019) High-performance flexible self-powered photodetector based on perovskite and low-temperature processed In_2S_3 nanoflake film. Adv Mater Interfaces 6:1801526

16. Hao D, Zou J, Huang J (2020) Recent developments in flexible photodetectors based on metal halide perovskite. InfoMat 2:139–154

17. Garner S, Glaesemann S, Li X (2014) Ultra-slim flexible glass for roll-to-roll electronic device fabrication. App Phys A 116:403–407

18. Garner SM, Li X, Huang M-H (2017) Introduction to flexible glass substrates. In: Flexible glass: enabling thin, lightweight, and flexible electronics, pp 3–34

19. Mei F, Sun D, Mei S, Feng J, Zhou Y, Xu J et al (2019) Recent progress in perovskite-based photodetectors: the design of materials and structures. Adv Phys-X 4:1592709

20. Lai Z, Meng Y, Zhu Q, Wang F, Bu X, Li F, Wang W, Liu C, Wang F, Ho JC (2021) High-performance flexible self-powered photodetectors utilizing spontaneous electron and hole separation in quasi-2D halide perovskites. Small 17:2100442

21. Fan X, Nie W, Tsai H, Wang N, Huang H, Cheng Y, Wen R, Ma L, Yan F, Xia Y (2019) PEDOT: PSS for flexible and stretchable electronics: modifications, strategies, and applications. Adv Sci 6:1900813

22. Alemu D, Wei H-Y, Ho K-C, Chu C-W (2012) Highly conductive PEDOT:PSS electrode by simple film treatment with methanol for ITO-free polymer solar cells. Energy Environ Sci 5:9662–9671

23. Nguyen TMH, Kim S, Bark CW (2021) Solution-processed and self-powered photodetector in vertical architecture using mixed-halide perovskite for highly sensitive UVC detection. J Mater Chem A 9:1269–1276

24. Imran M, Khan NA (2019) Perovskite phase formation in formamidinium–methylammonium lead iodide bromide $(FAPbI_3)_{1−x}(MAPbBr_3)_x$ materials and their morphological, optical and photovoltaic properties. Appl Phys A 125:1–9

25. Xie L-Q, Chen L, Nan Z-A, Lin H-X, Wang T, Zhan D-P et al (2017) Understanding the cubic phase stabilization and crystallization kinetics in mixed cations and halides perovskite single crystals. J Am Chem Soc 139:3320–3323

26. Jiang Q, Zhang L, Wang H, Yang X, Meng J, Liu H et al (2016) Enhanced electron extraction using SnO_2 for high-efficiency planar-structure $HC(NH_2)_2PbI_3$-based perovskite solar cells. Nat Energy 2:1–7

27. Xiao YY, Meng Y, Gao H, Chen Y, Meng Q, Bai Y et al (2020) Flexible perovskite solar cells fabricated by a gradient heat treatment process. Sustain Energy Fuels 4:824–831

28. Jiang Q, Chu Z, Wang P, Yang X, Liu H, Wang Y et al (2017) Planar-structure perovskite solar cells with efficiency beyond 21%. Adv mater 29:1703852

29. Bahtiar A, Rahmanita S, Inayatie Y (2017) Pin-hole free perovskite film for solar cells application prepared by controlled two-step spin-coating method. IOP Conf Ser: Mater Sci Eng 196:012037

30. Du T, Burgess CH, Kim J, Zhang J, Durrant JR, McLachlan MA (2017) Formation, location and beneficial role of PbI_2 in lead halide perovskite solar cells. Sustain Energy Fuels 1:119–126

31. Chen Y, Meng Q, Xiao Y, Zhang X, Sun J, Han CB et al (2019) Mechanism of PbI_2 in situ passivated perovskite films for enhancing the performance of perovskite solar cells. ACS Appl Mater Interfaces 11:44101–44108

32. Tonui P, Oseni SO, Sharma G, Yan Q, Mola GT (2018) Perovskites photovoltaic solar cells: an overview of current status. Renew Sust Energ Rev 91:1025–1044

33. Zhang W, Bi X, Zhao X, Zhao Z, Zhu J, Dai S et al (2014) Isopropanol-treated PEDOT: PSS as electron transport layer in polymer solar cells. Org Electron 15:3445–3451

34. Zhai Y, Li F, Guo M, Chen C (2017) Comparison of performance and stability of perovskite solar cells with $CuInS_2$ and PH1000 hole transport layers fabricated in a humid atmosphere. J Nanopart Res 19:1–9

35. Jiang F, Liu T, Zeng S, Zhao Q, Min X, Li Z et al (2015) Metal electrode-free perovskite solar cells with transfer-laminated conducting polymer electrode. Opt Express 23:A83–A91

36. Su L, Yang W, Cai J, Chen H, Fang X (2017) Self-powered ultraviolet photodetectors driven by built-in electric field. Small 13:1701687

37. Xie C, Yan F (2017) Flexible photodetectors based on novel functional materials. Small 13:1701822

38. Fang H, Hu W (2017) Photogating in low dimensional photodetectors. Adv Sci 4:1700323

39. Zhang T, Wang F, Zhang P, Wang Y, Chen H, Li J et al (2019) Low-temperature processed inorganic perovskites for flexible detectors with a broadband photoresponse. Nanoscale 11:2871–2877

40. Tran MH, Bae JS, Hur J (2022) Self-powered, transparent, flexible, and solar-blind deep-UV detector based on surface-modified TiO_2 nanoparticles. Appl Surf Sci 604:154528

41. Alluri NR, Purusothaman Y, Chandrasekhar A, Kim SJ (2018) Self-powered wire type UV sensor using in-situ radial growth of $BaTiO_3$ and TiO_2 nanostructures on human hair sized single Ti-wire. Chem Eng J 334:1729–1739

42. Chen WH, Ma CH, Hsieh SH, Lai YH, Kuo YC, Chen CH, Chang SP, Chang SJ, Horng RH, Chu YH (2022) High stability flexible deep-UV detector based on all-oxide heteroepitaxial junction. ACS Appl Electron Mater 4:3099–3106

43. He J, Wu J, Hu S, Shen H, Hu X (2019) A low-cost flexible broadband photodetector based on SnO_2/$CH_3NH_3PbI_3$ hybrid structure. Opt Mater 88:689–694

44. Cai S, Zuo C, Zhang J, Liu H, Fang X (2021) A paper-based wearable photodetector for simultaneous UV intensity and dosage measurement. Adv Funct Mater 31:2100026

45. Zheng Q, Huang J, Cao S, Gao H (2015) A flexible ultraviolet photodetector based on single crystalline MoO_3 nanosheets. J Mater Chem C 3:7469–7475

46. Zhang X, Li J, Yang W, Leng B, Niu P, Jiang X, Liu B (2019) High-performance flexible ultraviolet photodetectors based on AZO/ZnO/PVK/PEDOT:PSS heterostructures integrated on human hair. ACS Appl Mater Interfaces 11:24459–24467

Publisher's Note